

Stress-Strain Analysis and Visual Observation of Wheat Kernel Breakage During Roller Milling Using Fluted Rolls

Chaoying Fang¹ and Grant M. Campbell^{1,2}

ABSTRACT

Cereal Chem. 79(4):511–517

The endosperm and bran of a wheat grain have different mechanical properties and break differently under the same stresses. Stress-strain analysis was used to model the factors affecting wheat kernel breakage during milling using fluted rolls. The planes of principal compressive and tensile stress and the maximum shear stresses, along which the kernel is most likely to be broken, were calculated for a sharp-to-sharp roll disposition. With the occurrence of compressive stress in the horizontal direction and shear stress in the vertical direction, a kernel tends to break

along a principal tensile stress plane because the tensile strength of the endosperm is much smaller than its compressive strength. The model presented quantifies the mathematical relationship of three design and operational factors affecting the principal stresses and the maximum shear stresses: roll gap, differential, and roll diameter. High-speed video was used to observe wheat breakage events during milling; the results show consistency with the theoretical analysis.

The objective of milling is to open up the grain, scrape off as much endosperm from the bran skin as possible, and gradually grind the endosperm into flour, thus obtaining high yields of flour relatively free of bran contamination (Bass 1988; Sugden and Osborne 2001). In modern flour milling, conditioned wheat kernels are broken open using first-break roller mills, comprising pairs of counter-rotating fluted rolls operating under a speed differential of up to 2.7:1 with a small gap between the rolls. The fluted rolls open up the wheat kernel such that the bran particles tend to remain large while the endosperm particles are smaller, allowing bran and endosperm to be separated by size using plansifters. First-break roller milling produces a wide range of particles from <200 μm to >2,000 μm . Subsequent processes, typically four or more break passages, grading, purification, and eight or more reduction passages, mill and separate the endosperm and bran further. The particle-size distribution resulting from first-break roller milling directly affects the subsequent system arrangement and machine settings, and thus determines the effectiveness of the milling process (Smith 1944).

During comminution operations, both material properties and milling methods affect particle breakage (Scanlon and Lamb 1995). In first-break roller milling of wheat, the factors affecting breakage of wheat grains can thus be broadly classified into those arising from the physicochemical properties of the wheat (size distribution, moisture content, hardness) and those related to the design and operation of the milling equipment (Campbell et al 2001). The hardness of the wheat is the most important factor affecting milling performance (Pomeranz and Williams 1990). Hard wheat kernels initially shatter into large angular pieces, few fine particles are released, and bran is cleanly removed from the endosperm in the subaleurone region. In soft wheats, the fracture occurs through the contents of the endosperm cells, many fine particles are released during disruption, and more endosperm adheres to the bran, resulting in poor bran cleanup. Blakeney et al (1979) suggested that, in soft wheat endosperm, the air-filled spaces between the protein matrix and starch granules may act as a cushion, allowing the grain to deform but also transmitting the applied force hydrostatically through the endosperm. This may be the reason for the relatively large amounts of small particles arising from first-break roller milling of soft wheat.

Dobraszczyk (1994) measured fracture toughness of vitreous and mealy endosperm and concluded that the vitreous endosperm has higher fracture toughness than mealy endosperm because the former

has higher particle-matrix adhesion between starch granules and the protein matrix.

Wheat hardness also affects the breakage patterns of bran. During milling, shear forces are redirected through the endosperm of hard wheats to the bran and thus cause the bran to break, while in soft wheat, the shear forces are not redirected in this way and bran is less broken (Pomeranz and Williams 1990). The thickness of the bran layers is less influential in determining the milling behavior of wheat (Larkin et al 1951).

Glenn and coworkers (1991, 1992) used stress-strain analysis to investigate the mechanical properties of machined endosperm samples and bran strips from 31 common hard and soft wheat samples. They found that the compressive strength of wheat endosperm ranged from 11.6 to 61.3 MPa, while breakage strains were 2.71–7.11%, depending on the hardness of the wheat. The tensile strength of the endosperm was 1.74–5.18 MPa, an order of magnitude smaller than the compressive strength. Their study on the mechanical properties of wheat bran showed the bran to be nearly isotropic with no consistent differences in the mechanical properties of bran from hard or soft wheat samples. The tensile strength of bran was \approx 18–26 MPa and the strain to break was \approx 14–26%.

Arnold and Roberts (1966) used a photoelastic model to study the stress distributions in wheat grains under compressive loading between two flat rigid surfaces with the aim of specifying the critical loads at which the material fails. They concluded that under compression, the bran does not carry any of the applied load, serving only to contain the endosperm material. Breakage of wheat grains is therefore dominated by the fracture events occurring in the endosperm.

Because of the differences of the mechanical properties, endosperm and bran do not break in the same way under the same stresses. This results in the broad size distributions and varying bran-endosperm composition of first-break particles. This fact provides millers and milling engineers an opportunity to control the size distribution and composition through appropriate design and operation of the milling process. This requires a full understanding of the effects of fluted rolls on the breakage of wheat grains.

Studies on milling equipment, including roll design and operational settings, have long been reported for both fluted and smooth rolls. Niernberger and Farrell (1970) compared experimental results from fluted rolls with three different diameters of 152, 228, and 305 mm (6, 9 and 12 in.), and found that 228-mm rolls gave the lowest ash content. Creason (1975) believed larger diameter rolls, with their greater arc of contact, would be better for coarser reduction. McCorkle (1973) noted that roll spirals help to open up the wheat berry with a scissors-like motion, thus keeping the bran from being broken into smaller pieces. Gehle (1965) and Cleve and Will (1966) reported that the type of corrugation affects the ash content in the

¹ Satake Centre for Grain Process Engineering, Department of Chemical Engineering, UMIST, Manchester, M60 1QD, UK.

² Corresponding author. Phone: +44 (0)161 200 4472. Fax +44 (0)161 200 4399. E-mail: g.campbell@umist.ac.uk.

flour released from first-break roller milling. Schumacher (1967) summarized the effects of roll differential and feed rate on grinding, concluding that the differential affects the number of corrugations passing each other and thus helps to remove endosperm from the bran, and that at a given roll speed, a higher feeding rate results in a lower break release. Heide (1956) noted that the cutting action of the dull-to-dull or sharp-to-sharp disposition can be calculated in terms of the angles of the cutting edges, but the calculations reported omitted the relationships between compression and cutting actions and other factors such as roll gap and differential. Hsieh et al (1980) investigated the effects on first-break roller milling of roll differential, roll gap and roll speed. When the roll gap was reduced from 1.02 to 0.76 mm, the percentage of coarse fraction between 368 and 730 μm increased while the overtails $>730 \mu\text{m}$ reduced significantly. When roll differential was increased from 1.5:1 to 3:1, weight percentages of all fractions except the overtails increased.

Scanlon et al (1986, 1988), in their investigation of smooth roll grinding conditions on farina milling, found that flour starch damage increased with increased roll differential, while increasing compressive stress by reducing the roll gap did not affect starch damage of particles in the smaller size fraction ($<53 \mu\text{m}$). They attributed this to the relative contributions of compressive and shearing forces acting on the particles as they passed through the grinding zone.

The objective of this report is to identify the nature of the stresses and strains occurring during first-break roller milling and to relate these to breakage patterns of wheat kernels. A theoretical analysis of the stresses and strains experienced by a kernel during roller

milling using fluted rolls under a sharp-to-sharp disposition is presented. The effects of roll gap, differential, and roll diameter on the stress and strain are discussed. The results of this analysis are compared with high-speed video recordings of wheat breakage events.

STRESS AND STRAIN ANALYSIS OF A WHEAT KERNEL BETWEEN TWO ROLLS

Milling Using Smooth Rolls

Previous work (Austin et al 1980, 1981; Haque 1991) studied the situation of a particle being drawn into the nip of smooth rolls counter-rotating at the same speed. In these studies, the particle was assumed to be spherical, as shown in Fig. 1, and the conditions of the particle to be drawn into the roll nip were given as

$$F \cos \alpha \geq N \cdot \sin \alpha \quad (1)$$

or

$$\mu \geq \tan \alpha \quad (2)$$

where N is normal force, F is frictional force, μ is the static coefficient of friction (such that $F = \mu N$) and 2α is the nip angle. The static coefficient of friction, μ , is affected by the surface condition of rolls, and α is determined by roll diameter, particle diameter, and the roll gap

$$\alpha = \cos^{-1}(d + G)/(D + d) \quad (3)$$

where d is the roll diameter, G is the roll gap, and D is the particle diameter. Equation 3 indicates that large d and G or smaller D makes the particle more easily drawn into the roll nip. Once the particle is drawn into the roll nip, the strain increases as the particle goes toward the roll nip, and the particle is crushed provided

$$\sigma = E\varepsilon \geq \sigma_c$$

where σ and ε are the stress and strain of the particle, E is the elastic modulus, and σ_c is the compressive strength of the particle. Using smooth rolls operating at the same speed, wheat kernels would be flattened and may shatter, but the desired separation of bran and endosperm would not occur. If two rolls were to rotate at different speeds, shear stress would be induced in the kernels. However, the shear action may not be sufficient to cause the kernel to break because it would rely on the friction from the smooth rolls.

Strains Caused by Fluted Rolls Rotating with a Differential Speed

Fluted rolls are used in first-break roller milling with the two rolls counter-rotating at different speeds. Figure 2 shows a typical profile of the flute in which β_s and β_d are sharp and dull working angles, respectively.

Depending on the orientation of the two rolls, there are four possible roll dispositions: sharp-to-sharp (S-S), sharp-to-dull (S-D), dull-to-sharp (D-S), and dull-to-dull (D-D) (Fig. 3), where $n_1 > n_2$. Different roll dispositions will result in different stress distributions and, thus, different breakage patterns of the kernels.

Fluted rolls make it possible to constrain the movement of the kernel and to introduce shear stresses to the kernel. Using S-S as an example, the particle can be considered to be stationary with respect to the slow (right-hand side) roll (Fig. 4). For simplicity it is assumed that the particle is in contact with each roll at a single point (A and C for the fast roll and slow roll, respectively) at any moment before breakage. This is supported by observation using high-speed video. The rotation of the fast roll causes both compressive and shear deformation of the particle. The speeds of the fast roll and slow roll are n_1 and n_2 , respectively. The distance between the two contact points A and C is W ; the vertical distance between the two points is S ; and the horizontal distance is H . If the centers of the fast roll and slow roll are at O_1 and O_2 respectively, α_1 is the angle $\angle AO_1O_2$ and α_2 is the angle $\angle CO_2O_1$.

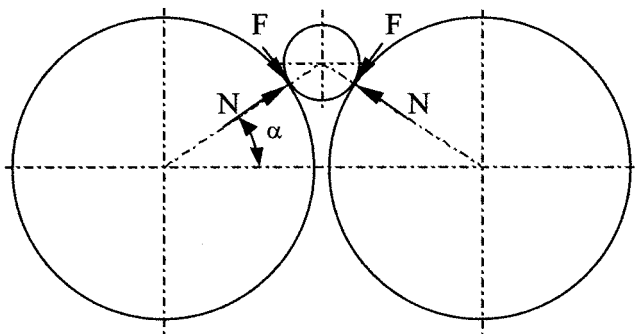


Fig. 1. A spherical particle engaged between two smooth rolls.

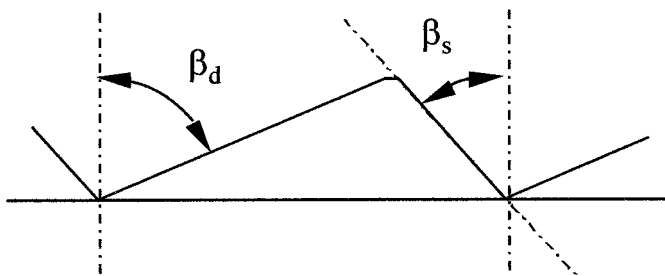


Fig. 2. Flute profile of a first-break milling roll.

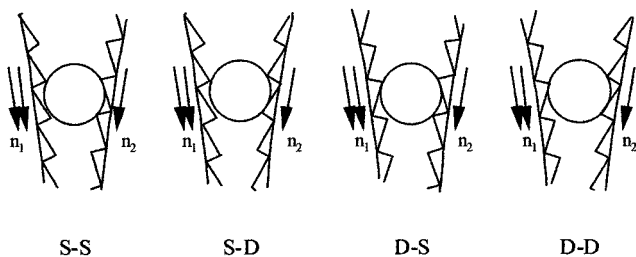


Fig. 3. Four types of roll disposition: sharp-to-sharp (S-S); sharp-to-dull (S-D); dull-to-sharp (D-S); and dull-to-dull (D-D).

Then from simple geometry

$$S = R(\sin \alpha_1 - \sin \alpha_2) \quad (5)$$

$$H = (2R + G) - R(\cos \alpha_1 + \cos \alpha_2) \quad (6)$$

and

$$W^2 = S^2 + H^2 \quad (7)$$

where G is the roll gap and R is the roll radius. Assuming there is no slippage between the particle and rolls and that the particle is homogeneous, with a small rotating angle of $d\alpha_1$, the particle will be deformed. Thus the changes ΔW and ΔS can be calculated by differentiating Equations 5, 6, and 7:

$$\begin{aligned} 2WdW &= 2S\left(\frac{\partial S}{\partial \alpha_1}d\alpha_1 + \frac{\partial S}{\partial \alpha_2}d\alpha_2\right) + 2H\left(\frac{\partial H}{\partial \alpha_1}d\alpha_1 + \frac{\partial H}{\partial \alpha_2}d\alpha_2\right) \\ &= 2R\left[S(\cos \alpha_1 - \frac{1}{\Delta n}\cos \alpha_2) + H(\sin \alpha_1 + \frac{1}{\Delta n}\sin \alpha_2)\right]d\alpha_1 \end{aligned} \quad (8)$$

where $d\alpha_1$ and $d\alpha_2$ are the change of α_1 and α_2 , and Δn is the differential in which $d\alpha_2 = \Delta n \bullet d\alpha_1$. Thus, the compressive strain ϵ_x can be expressed as

$$\begin{aligned} \epsilon_x &= \frac{dW}{W} \\ &= \frac{R\left[S(\cos \alpha_1 - \frac{1}{\Delta n}\cos \alpha_2) + H(\sin \alpha_1 + \frac{1}{\Delta n}\sin \alpha_2)\right]d\alpha_1}{S^2 + H^2} \end{aligned} \quad (9)$$

Similarly, from Equation 5:

$$\begin{aligned} dS &= R(\cos \alpha_1 d\alpha_1 - \cos \alpha_2 d\alpha_2) \\ &= R(\cos \alpha_1 - \frac{1}{\Delta n}\cos \alpha_2) d\alpha_1 \end{aligned} \quad (10)$$

Then the shear strain γ_{xy} can be expressed as

$$\begin{aligned} \gamma_{xy} &= \frac{dS}{H} \\ &= \frac{R(\cos \alpha_1 - \frac{1}{\Delta n}\cos \alpha_2) d\alpha_1}{(2R + G) - R(\cos \alpha_1 + \cos \alpha_2)} \end{aligned} \quad (11)$$

Equations 9 and 11 show the factors affecting ϵ_x and γ_{xy} at different α_1 and α_2 , including R , G and Δn . The α_1 and α_2 indicate the position of a particle in the grinding zone, which depends on the size of the particle, roll radius, and the gap between rolls. The α_2 is slightly smaller than α_1 because the particle is seated on the slow roll while the fast roll affects the particle from behind; the difference between α_1 and α_2 becomes smaller as particle size reduces. Because there is no compression in the y-axis direction, ϵ_y is ignored, $\epsilon_y = 0$.

Figures 5 and 6 show the relationships described by Equations 9 and 11, showing the total changes in ϵ_x and γ_{xy} as α_1 changes from its initial value down to a value equal to α_2 . In other words, the calculated values indicate the strains experienced when the fast roll moves from point A to a point between B and C (Fig. 4). Note

that the “-” sign in Fig. 5 indicates compressive strains, and in Fig. 6 it indicates that the shear is in the direction of α_1 reducing. For simplicity, it was assumed that no slippage occurs and that the line linking the two contact points A and C passes through the center of the particle, thus $W = D$, where D is the diameter of the particle. This means that for different gaps (Figs. 5A and 6A) or different roll diameters (Figs. 5B and 6B), a given initial value of α_1 corresponds to different initial particle sizes. A larger particle will make contact with the fast roll earlier and will thus have a larger initial value of α_1 . It will be compressed to a greater extent and therefore experience larger compressive and shear strains. The compressive and shear strains indicate the total strain that a particle that makes initial contact with the fast roll at an angle of α_1 would experience once α_1 had decreased to a value equal to α_2 .

Comparing Figs. 5 and 6, we can make four hypotheses. 1) For a given value of α_1 , the shear strain is larger than the compressive strain under the same conditions. 2) A smaller roll gap produces larger strains for both the compressive strain and the shear strain, but roll gap has a slightly larger effect on the shear strain. 3) Larger diameter rolls generate smaller values for both the compressive strain and the shear strain. This is because a larger diameter gives a smaller curvature of the roll surface, thus the change of horizontal distance as the rolls counter-rotate is also smaller. However, larger rolls have a longer grinding zone, so are likely to generate a larger number of breakage events. Therefore, larger rolls may ultimately give more breakage overall than smaller rolls. 4) Shear strain arises from the action of roll differential. A larger differential gives a larger shear strain, but the compressive strain remains constant (Fig. 5C) where compressive strains are the same for various differentials and the curves coincide. The shear strain increases to a lesser extent with further increases in the differential.

The above analysis is based on a spherical particle. For other shapes such as cylinders or wheat kernels under various orientations, the analysis is still valid because the generated strains depend only on the distance (W) between the two initial contact points, A and C.

Planes of Principal Stress and Maximum Shear Stress

Based on the calculated compressive and shear strains, the principal strains ϵ_1 and ϵ_2 , the maximum shear strain γ_{max} and the planes along which they occur can be calculated by (Gere and Timoshenko 1984)

$$\epsilon_{1,2} = -\frac{\epsilon_x}{2} \mp \sqrt{\left(\frac{-\epsilon_x}{2}\right)^2 + \left(\frac{\gamma_{xy}}{2}\right)^2} \quad (12)$$

$$\frac{\gamma_{max}}{2} = \sqrt{\left(\frac{-\epsilon_x}{2}\right)^2 + \left(\frac{\gamma_{xy}}{2}\right)^2} \quad (13)$$

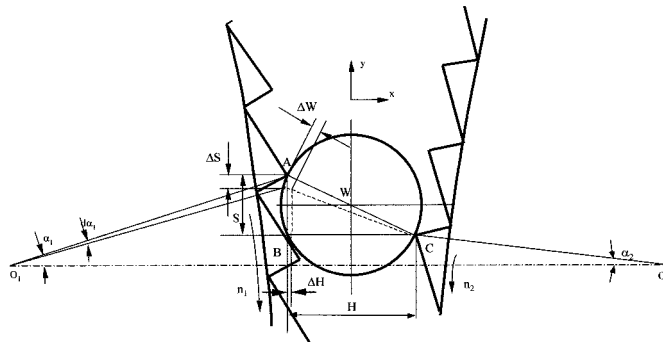


Fig. 4. A spherical particle engaged between two counter-rotating fluted rolls with sharp-to-sharp (S-S) disposition showing the forces acting on the particle. Note that the positions of O_1 and O_2 are not to scale.

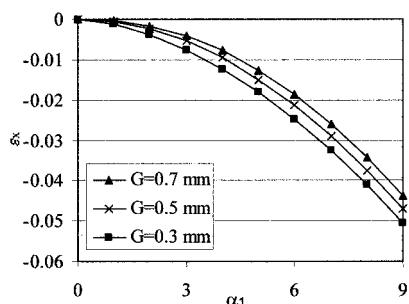
The ε_1 and ε_2 , and γ_{\max} can be illustrated in a Mohr's circle. Fig. 7 shows a Mohr's circle construction for $\alpha_1 = 9^\circ$, $D = 4$ mm, $R = 125$ mm, $G = 0.5$ mm, $\Delta n = 2.7$, and $d\alpha_1 = \alpha_1 - \alpha_2 = 0.25^\circ$. Points A and B on the circle represent strains on the planes in the x -axis and the y -axis directions, respectively. The principal strains are at points P_1 and P_2 representing two planes. The angle between the plane P_1 and the x -axis can be expressed as

$$\theta_{P_1} = \frac{1}{2} \tan^{-1} \left(\frac{\gamma_{xy}}{-\varepsilon_x} \right) \quad (14)$$

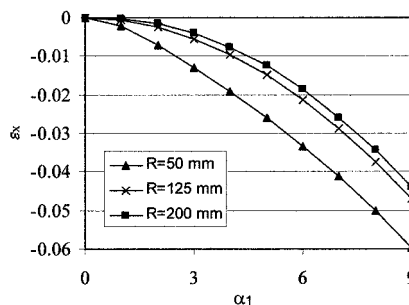
The principal strain at P_2 is actually a tensile strain, which is in a plane perpendicular to the principal compressive stress, $\theta_{P_2} = \theta_{P_1} + 90^\circ$. The maximum shear strains are at orthogonal planes given by $\theta_{S,S'} = \theta_{P_1} \pm 45^\circ$. Equation 12 shows that with the existence of γ_{xy} , $\varepsilon_2 > 0$, which means the ε_2 is a tensile strain.

Figure 8 illustrates the positions of these planes in the S-S disposition when α_1 is 9° , that is, where the kernel just enters the grinding zone.

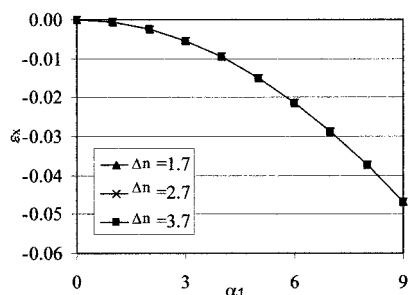
With a particle that makes initial contact further into the grinding zone, corresponding to a smaller α_1 , the positions of the planes



A $R=125$ mm, $\Delta n=2.7$



B $G=0.5$ mm, $\Delta n=2.7$



C $R=125$ mm, $G=0.5$ mm.
Note that the three curves coincide.

Fig. 5. Effect of (A) roll gap; (B) roll diameter; and (C) differential on the compressive strain experienced by a wheat kernel during breakage using fluted rolls under sharp-to-sharp (S-S) disposition.

with the principal strains and the maximum shear strain will change. Figure 9 shows that the angles of these planes rotate clockwise as α_1 decreases.

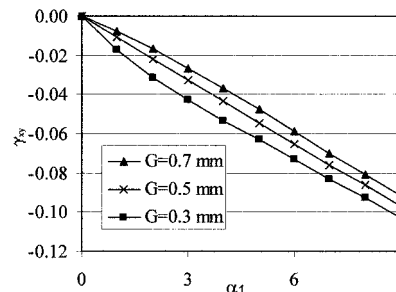
Assuming Hooke's law holds for the material, the relevant principal stresses and the maximum shear stresses can also be calculated by

$$\sigma_1 = \frac{E}{1-\nu^2} (\varepsilon_1 + \nu\varepsilon_2) \quad (15)$$

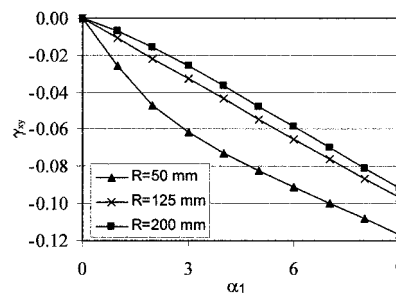
$$\sigma_2 = \frac{E}{1-\nu^2} (\varepsilon_2 + \nu\varepsilon_1) \quad (16)$$

$$\tau_{\max} = G\gamma_{\max} \quad (17)$$

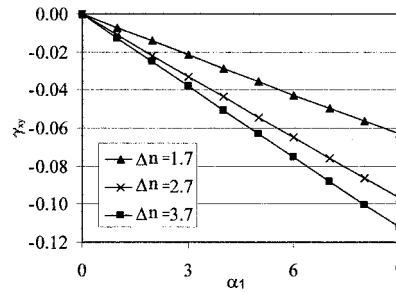
where σ_1 and σ_2 are the principal stresses in orthogonal planes P_1 and P_2 , respectively, τ_{\max} is the maximum shear stress in orthogonal planes S and S' , ν is Poisson's ratio, E is the modulus of elasticity, and G is the shear modulus of elasticity. A particle will break along the plane where its principal stress or maximum shear stress exceeds its compressive, tensile, or shear strength, depending on which reaches the critical stress first. If the strength properties



A $R=125$ mm, $\Delta n=2.7$



B $G=0.5$ mm, $\Delta n=2.7$



C $R=125$ mm, $G=0.5$ mm

Fig. 6. Effect of (A) roll gap; (B) roll diameter; and (C) differential on the shear strain experienced by a wheat kernel during breakage using fluted rolls under sharp-to-sharp (S-S) disposition.

of a wheat kernel are known, the plane along which a kernel will break can be predicted using Equations 15–17; the breakage plane will be one of those shown in Fig. 8 if the mechanical properties of the kernel are homogeneous. According to Glenn and coworkers (1991, 1992), the endosperm is approximately one order of magnitude stronger under compression than tension for the same wheat sample (although the shear strength is not reported here). Therefore, the kernel is most likely to be broken initially along P_2 by tensile stress. However, the tensile stress is generated by the shear stress. Equation 12 and the Mohr's circle construction in Fig. 7, show that principal strain ϵ_2 will be smaller for the same compressive strain ϵ_x if the shear strain γ_{xy} is smaller.

MATERIALS AND METHODS

A Kodak EK high-speed video system was used to observe wheat kernel breakage. The system is capable of capturing up to 6000 frames per second. The pictures are recorded onto a tape and can be printed with a thermal video printer. A speed of 2000 frames per second was used in this work to get high-quality pictures. The video camera was focused on the grinding zone of the fluted rolls on the Satake STR-100 test roller mill. The STR-100 test roller mill is a single-pass, fully variable test mill that uses full-scale rolls (250 mm diameter, 100 mm length) to mimic commercial flour milling operations. First-break rolls with 10.5 flutes per inch were used under a sharp-to-sharp disposition. The speed of the fast roll was set at 100 rpm, much slower than the 600 rpm more typical of commercial practice, to allow capture of the breakage events on video. Results reported by Hsieh et al (1980) indicate that the

effect of roll speed on kernel breakage is very small compared with roll gap and differential. The differential was set at 2.7 and the roll gap was 0.6 mm. Consort (a soft wheat from the 1999 UK harvest, 12.7% protein, db; 79.4 kg/hL), conditioned overnight to 16% moisture content, wb, was used for the observations.

RESULTS

Figures 10–12 show some typical examples of wheat breakage events, selected from more than 30 similar events recorded and many more observed. Figure 10 shows a kernel that enters the grinding zone longitudinally. In Fig. 10A, the two arrows show the initial contacting points between the kernel and flutes from both rolls; α_1 is $\approx 7^\circ$ and the length of grinding zone is 15 mm. Figure 10B shows the first fracture of the kernel 0.5 msec after the initial contact shown in Fig. 10A. The fracture plane is $\approx 60^\circ$ from the vertical direction, similar to the angle of the principal tensile fracture plane shown in Fig. 8B. After 2.5 msec, the kernel has undergone a second fracture by the flute following the initial contacting flute of the fast roll (Fig. 10C). Figure 10D shows that after 4.5 msec, the latter part of the kernel experiences a further breakage by the third flute, meanwhile the entire kernel has started to disintegrate under the compressive crushing forces. By 7.5 msec (Fig. 10E), the broken particles have reached the roll nip. Because they have been disintegrated, these small particles are no longer held tightly between the two rolls, and relative movement occurs. The initial contacting points have moved away from the broken particles and the particles spread over the length between the two initial contacting points.

Figures 11 shows a similar example. Figure 11A shows the two initial contacting points. Figure 11B shows the kernel is broken into two parts by the first flute after 0.5 msec, again with an angle from the vertical of $\approx 60^\circ$. After 1.5 msec (Fig. 11C), the second fragment is further broken into two parts by the second flute. Figure 11D shows that after 3 msec, the trailing fragment is broken again by

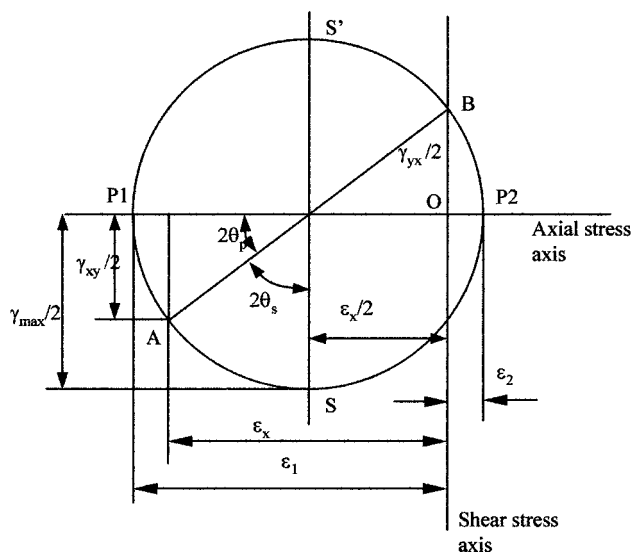


Fig. 7. Mohr's circle construction to illustrate the positions of the planes of principal and maximum shear strain.

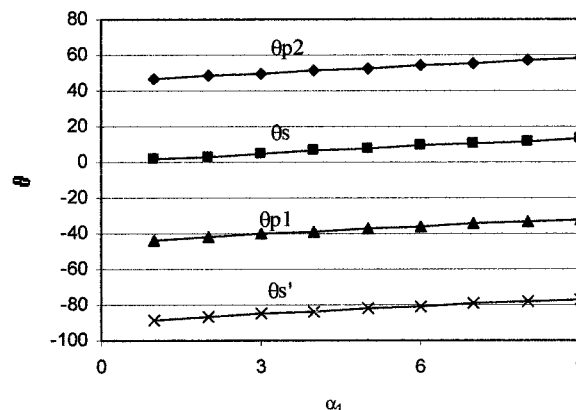


Fig. 9. Directions of principal strain and maximum shear strain.

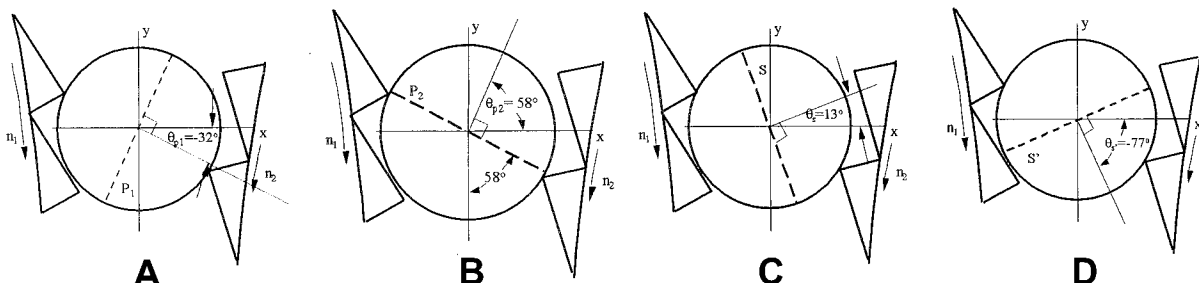


Fig. 8. Positions of planes with principal strains and maximum shear strains in sharp-to-sharp (S-S) disposition when α_1 is 9° . (A) Principal compressive strain; (B) principal tensile strain; (C) and (D) maximum shear strains.

the third flute. By 7 msec (Fig. 11E), the disintegrated particles have spread between two initial points. Thus, the endosperm is released over a larger area.

Figure 12 shows a kernel entering the grinding zone laterally. In this case, the mechanical properties of the kernel cross-section are not homogenous because of the presence of the crease, which is more likely to be broken first (Dobraszczyk 1994). Figure 12A shows initial contact. Figure 12B shows breakage along the crease by the initial contacting flute after 1.5 msec. The two separated parts of the kernel are then each broken into two more fragments after 4 msec.

The style of the kernel breakage in these examples shows that once the kernel breaks, its broken parts are separated, which means

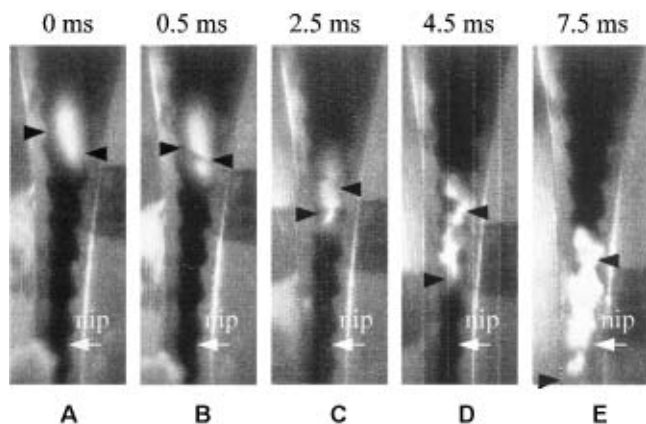


Fig. 10. Pictures from high-speed video showing kernel breakage. Left surface is the fast roll and right surface is the slow roll. Black arrows indicate points of initial contact.

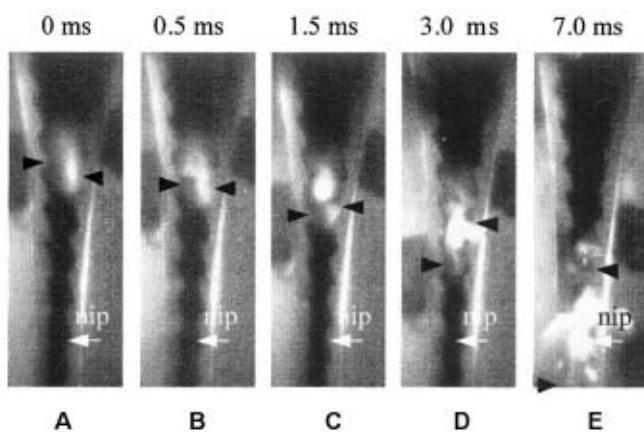


Fig. 11. Example of kernel breakage similar to that in Fig. 10.

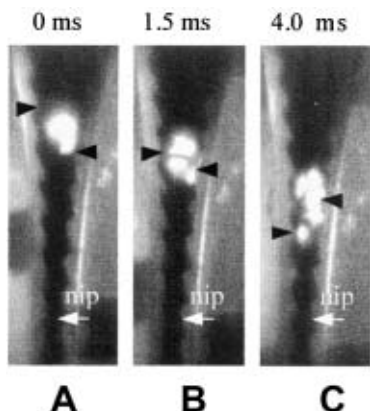


Fig. 12. Pictures from high-speed video showing kernel breakage when the kernel enters the grinding zone laterally.

the bran has been broken together with the endosperm. It can also be noted that there is no slippage between the kernels and the flutes, although after initial breakage additional following flutes from the fast roll become involved in subsequent breakage events.

CONCLUSIONS

Stress-strain analysis has established equations that highlight the fracture mechanics principles determining kernel breakage during roller milling in terms of particle size, roll gap, roll differential, and roll diameter. The combination of compressive stress applied in the horizontal direction and shear stress applied in the vertical direction means that a wheat kernel is most likely to break along the plane corresponding to the principal tensile stress, because of the weak tensile strength of endosperm compared with its compressive strength. High-speed video pictures of wheat breakage during first-break roller milling support these conclusions.

ACKNOWLEDGMENTS

This work was funded under EPSRC grant GR/M49939. We are also grateful for the loan of the high-speed video system from the EPSRC Equipment Pool Loan Scheme. The Satake Corporation of Japan is gratefully acknowledged for its support of these studies.

LITERATURE CITED

- Arnold, P. C., and Roberts, A. W. 1966. Stress distributions in loaded wheat grains. *J. Agric. Eng. Res.* 11:38-43.
- Austin, L. G., van Orden, D. R., and Perez, J. W. 1980. A preliminary analysis of smooth roll crushers. *Int. J. Mineral Proc.* 6:321-336.
- Austin, L. G., van Orden, D., McWilliams, B., and Perez, J. W. 1981. Breakage parameters of some materials in smooth roll crushers. *Powder Technol.* 28:245-251.
- Bass, E. J. 1988. Wheat flour milling. Pages 1-68 in: *Wheat: Chemistry and Technology*, Vol. 2. 3rd Ed. Y. Pomeranz, ed. Am. Assoc. Cereal Chem.: St. Paul, MN.
- Blakeney, A. B., Almgren, G., and Jacob, E. H., 1979. Analysis of first break milling of hard and soft wheats. *Milling Feed Fert.* 162(9):22-28.
- Campbell, G. M., Bunn, P. J., Webb, C., and Hook S. C. W. 2001. On predicting roller milling performance. II. The breakage function. *Powder Technol.* 115:243-255.
- Cleve, H., and Will, F. 1966. Research with the help of the Varioroll. *Cereal Sci. Today* 11:128-132.
- Creason, H. 1975. Grinding and corrugating rolls. *Bull. Assoc. Oper. Millers.* November: 3569-3570.
- Dobraszczyk, B. J. 1994. Fracture mechanics of vitreous and mealy wheat endosperm. *J. Cereal Sci.* 19:273-282.
- Gehle, H. 1965. The Miag "Vario" rollstand—Design and purpose. *Bull. Assoc. Oper. Millers.* November: 2861-2862.
- Gere, J. M., and Timoshenko, S. P. 1984. *Mechanics of Materials*, 2nd Ed. Wadsworth: Belmont, CA.
- Glenn, G. M., and Johnston, R. K. 1992. Moisture-dependent changes in the mechanical properties of isolated wheat bran. *J. Cereal Sci.* 15:223-236.
- Glenn, G. M., Younce, F. L., and Pitts, M. J. 1991. Fundamental physical properties characterizing the hardness of wheat endosperm. *J. Cereal Sci.* 13:179-194.
- Haque, E. 1991. Application of size reduction theory to roller mill design and operation. *Cereal Foods World* 36:368-375.
- Heide, F. M. 1956. Roll corrugation. *Bull. Assoc. Oper. Millers.* December: 2292-2294.
- Hsieh, F. H., Martin, D. G., Black, H. C., and Tipples, K. H. 1980. Some factors affecting the first break grinding of Canadian wheat. *Cereal Chem.* 57:217-223.
- Larkin, R. A., MacMasters, M. M., Wolf, M. J., and Rist, C. E. 1951. Studies on the relation of bran thickness to millability of some Pacific Northwest wheats. *Cereal Chem.* 28:247-258.
- McCorkle, F. D. 1973. Development and operation of the modern roller mill. *Bull. Assoc. Oper. Millers.* May: 3362-3364.
- Niernberger, F. F., and Farrell, E. P. 1970. Effects of roll diameter and speed on first break grinding of wheats. *Bull. Assoc. Oper. Millers.* January: 3154-3158.

- Pomeranz, Y., and Williams, P. C. 1990. Wheat hardness: Its genetic, structural, and biochemical background, measurement, and significance. Pages 471-548 in: *Advances in Cereal Science and Technology*, Vol. 10. Y. Pomeranz, ed. Am. Assoc. Cereal Chem.: St. Paul, MN.
- Scanlon, M. G., and Dexter, J. E. 1986. Effect of smooth roll grinding conditions on reduction of hard red spring wheat farina. *Cereal Chem.* 63:431-435.
- Scanlon, M. G., Dexter, J. E., and Biliaderis, C. G. 1988. Particle-size related physical properties of flour produced by smooth roll reduction of hard red spring wheat farina. *Cereal Chem.* 65:486-492.
- Scanlon, M. G., and Lamb, J. 1995. Fracture mechanism and particle shape formation during size reduction of a model food material. *J. Mater. Sci.* 30:2577-2583.
- Schumacher, F. 1967. Technical aspects of grinding with roller mills. *Bull. Assoc. Oper. Millers*. January: 2956-2957.
- Smith, L. 1944. *Flour Milling Technology*. 3rd Ed. Northern: Liverpool, England.
- Sugden, T. D., and Osborne, B. G. 2001. Wheat flour milling. Pages 140-181 in: *Cereals and Cereal Products: Chemistry and Technology*. D. A. V. Dendy and B. J. Dobraszczyk, eds. Aspen Publishers: New York.

[Received June 11, 2001. Accepted January 31, 2002.]